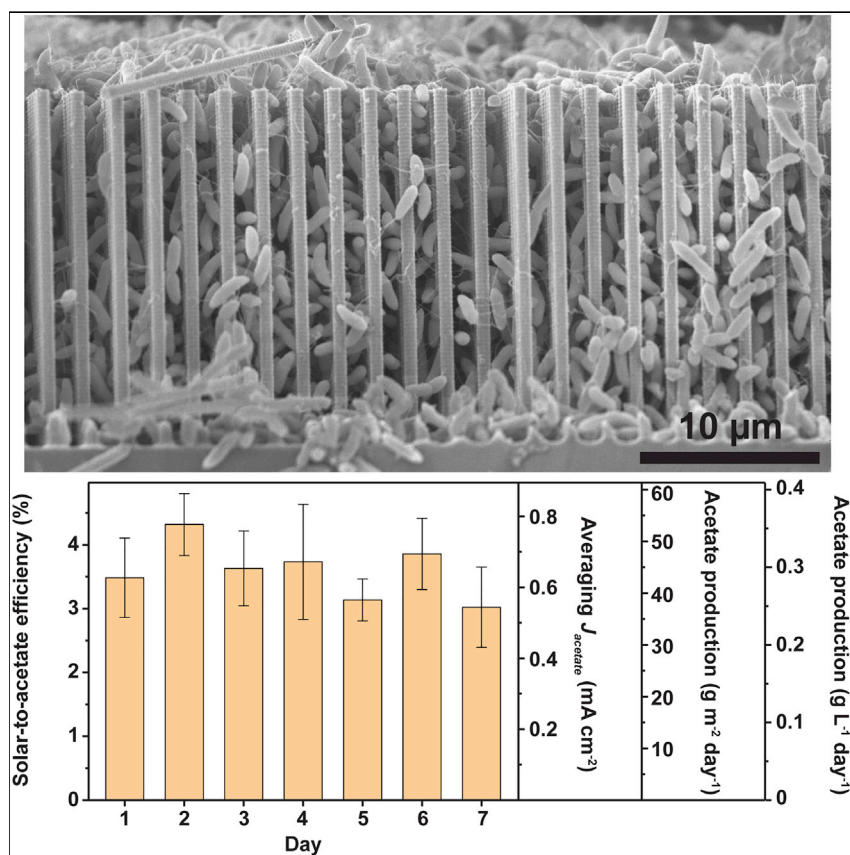


Report

Close-Packed Nanowire-Bacteria Hybrids for Efficient Solar-Driven CO₂ Fixation

Bioelectrochemical CO₂-reducing rate at high potential was limited by poor bacteria-nanowire interface resulting from an inhospitable alkaline local environment. Tuning the bulk electrolyte pH and increasing its buffering capacity mitigated this issue and supported the formation of a close-packed nanowire-bacteria cathode. The resulting close-packed biohybrid operated with a CO₂-reducing current density of 0.65 ± 0.11 mA cm⁻² at ~ -1.2 V versus standard hydrogen electrode and enabled solar-powered CO₂ fixation with solar-to-acetate efficiency of $\sim 3.6\%$ over 1 week.

Yude Su, Stefano Cestellos-Blanco, Ji Min Kim, ..., Hao Zhang, Yuhong Cao, Peidong Yang

p_yang@berkeley.edu

HIGHLIGHTS

Close-packed bacteria-nanowire hybrids achieved

Microbial CO₂-reducing current density boosted to 0.65 mA cm⁻²

COMSOL simulation explains the nanowire-cell interactions under different pH conditions

A 3.6% solar-to-acetate efficiency realized over 1 week

Report

Close-Packed Nanowire-Bacteria Hybrids for Efficient Solar-Driven CO₂ Fixation

Yude Su,^{1,6} Stefano Cestellos-Blanco,^{2,6} Ji Min Kim,^{2,6} Yue-xiao Shen,¹ Qiao Kong,¹ Dylan Lu,^{1,3} Chong Liu,⁵ Hao Zhang,¹ Yuhong Cao,¹ and Peidong Yang^{1,2,3,4,7,*}

SUMMARY

Microbial electro- and photo-electrochemical CO₂ fixation, in which CO₂-reducing microorganisms are directly interfaced with a cathode material, represent promising approaches for sustainable fuel production. Although considerable efforts have been invested to optimize microorganism species and electrode materials, the microorganism-cathode interface has not been systematically studied. Here, investigation of the interface allowed us to optimize the CO₂-reducing rate of silicon nanowire/*Sporomusa ovata* system. Tuning the bulk electrolyte pH and increasing its buffering capacity supported the formation of a close-packed nanowire-bacteria cathode. Consequently, the resulting close-packed biohybrid achieved a CO₂-reducing current density of $\sim 0.65 \text{ mA cm}^{-2}$. When coupled with a photovoltaic device, our system enabled solar-to-acetate production with $\sim 3.6\%$ efficiency over 7 days.

INTRODUCTION

Interfacing living cells and inorganic materials has enabled the development of diverse technologies including, but not limited to, gene editing,^{1,2} biosensing,^{3,4} and microbial fuel cells.^{5,6} Notably, microorganisms have been introduced as “living” catalysts to the field of catalytic CO₂ fixation.^{7–13} These microorganisms, principally chemoautotrophic bacteria, have metabolic pathways that can fix CO₂ into multi-carbon products.¹⁴ Biohybrid CO₂-fixing systems, particularly those driven by renewable solar energy, represent a promising strategy for sustainable CO₂-to-chemical conversion.¹⁵ The use of time-evolved living biocatalysts allows for high product selectivity, catalyst regeneration, and long-term operation.¹⁶ Remarkably, several of these microorganisms accept extracellular charge transfer and can be directly interfaced with a cathode to carry out CO₂ fixation.^{11–13} Different strategies have been employed to improve the performance of these hybrid systems, such as optimization of electrode geometry,¹⁷ electrode surface engineering,¹⁸ bacteria adaptation,^{19,20} and enrichment.²¹ In particular, our group has developed a photoactive and high-surface-area silicon (Si) nanowire electrode that allows for unassisted solar-to-chemical production when paired with acetogen *Sporomusa ovata* (*S. ovata*).¹³ The high surface area of the Si nanowire electrode²² allows for greater bacteria-electrode interface and thus enhanced charge transfer rate. However, the CO₂-reducing current of biohybrid systems mediated by direct charge transfer is typically lower than that of electrochemical systems composed of purely inorganic catalysts.^{23,24}

Previous work has proposed that the bioinorganic interface is a key determinant of the CO₂-reducing rate.¹⁸ Nevertheless, the dependence of the bioinorganic interface on electrochemical operational parameters, including applied overpotential

Context & Scale

Bioinorganic interface is a key determinant for microbial catalytic CO₂ fixation. However, the correlation between bioinorganic interface and CO₂-conversion efficiency has not been systematically studied as a function of operational parameters. Here, investigation of the microorganism-cathode interface allowed us to boost the CO₂-reducing rate in a silicon nanowire/*Sporomusa ovata* system. We found that the CO₂-reducing rate at high potential was limited by poor bacteria-nanowire interface resulting from an inhospitable alkaline local environment. Tuning the bulk electrolyte pH and increasing its buffering capacity mitigated this issue and facilitated the formation of a close-packed nanowire-bacteria cathode. The resulting close-packed biohybrid achieved a CO₂-reducing current density of $0.65 \pm 0.11 \text{ mA cm}^{-2}$. Our system enabled solar-powered CO₂ fixation with solar-to-acetate efficiency of $\sim 3.6\%$ over 1 week.

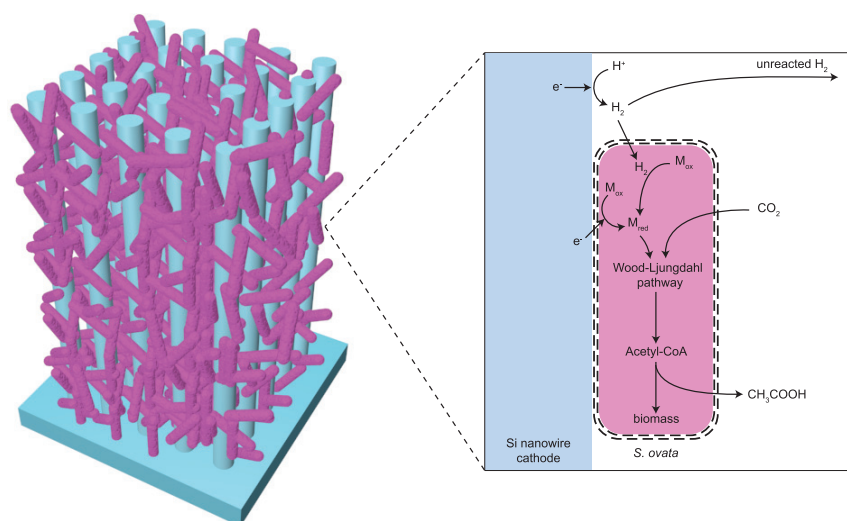


Figure 1. Schematics of the Close-Packed Nanowire-Bacteria Hybrid System (Left) and the Reaction Pathway (Right)

The electrons are transferred (via either direct pathway^{14,43,44} or H_2 -mediated pathway^{7,9,10}) from the Si nanowire cathode to *S. ovata* to generate the intracellular reducing equivalents (M_{red}). The reducing equivalents are finally passed on to the Wood-Ljungdahl pathway to produce acetate and biomass.

(η), biocatalyst loading, and electrolyte pH, is poorly understood. Here, we boosted the CO_2 -reducing rate of our model Si nanowire/*S. ovata* platform by establishing a robust bacteria-nanowire interface (Figure 1). First, we found that the CO_2 -reducing rate at high η was limited by poor bacteria-nanowire interface resulting from an inhospitable alkaline local environment. Second, tuning the bulk electrolyte pH mitigated the increase in local pH, which strengthened the bioinorganic interface. Additionally, this supported higher biocatalyst loading on the nanowire electrode, forming a close-packed nanowire-bacteria cathode. The resulting close-packed bio-hybrid operated with CO_2 -reducing current density ($J_{acetate}$) of $0.65 \pm 0.11 \text{ mA cm}^{-2}$ at $\sim -1.2 \text{ V}$ versus standard hydrogen electrode (SHE), with a faradic efficiency of acetate ($FE_{acetate}$) of $\sim 80\%$. When coupled with a photovoltaic device, our system enabled solar-powered CO_2 fixation with solar-to-acetate efficiency of $\sim 3.6\%$ and an average daily acetate production rate of 44.3 g m^{-2} or 0.3 g L^{-1} over 1 week.

RESULTS AND DISCUSSION

Liu et al. previously demonstrated that Si nanowire arrays with a large surface area could be used to accommodate electro-trophic *S. ovata*.¹³ Reducing equivalents generated from the light-harvesting electrodes powered *S. ovata* acetogenesis and thus, enabled the conversion of CO_2 into extracellular acetate. In order to focus our scope on the bioinorganic interface and separate it from limitations of the semiconductor-based light-harvesting process, we used highly doped conductive p^+ Si nanowire arrays as the cathode material and platinum (Pt) wire as the counter electrode in lieu of a TiO_2 photoanode. Initially, established inorganic phosphate-buffered media^{12,18} was used as the electrolyte (initial pH 7.2), and an *S. ovata* suspension (4% v/v at OD_{545} of 0.38; Figure S1) was inoculated into the cathodic chamber of the electrochemical cell (Experimental Procedures). With this setup, we investigated the influence of the applied η on acetate production. At the onset of the electrochemical operation, we observed that *S. ovata* was sparsely distributed within the nanowire arrays (Figure 2A) as each wire holds an average of ~ 2.6 cells (Figure S2).

¹Department of Chemistry, University of California, Berkeley, Berkeley, CA 94720, USA

²Department of Materials Science and Engineering, University of California, Berkeley, Berkeley, CA 94720, USA

³Materials Sciences Division, Lawrence Berkeley National Laboratory, Berkeley, CA 94720, USA

⁴Kavli Energy Nanosciences Institute, Berkeley, CA 94720, USA

⁵Department of Chemistry and Biochemistry, University of California, Los Angeles, Los Angeles, CA 90095, USA

⁶These authors contributed equally

⁷Lead Contact

*Correspondence: p_yang@berkeley.edu
<https://doi.org/10.1016/j.joule.2020.03.001>

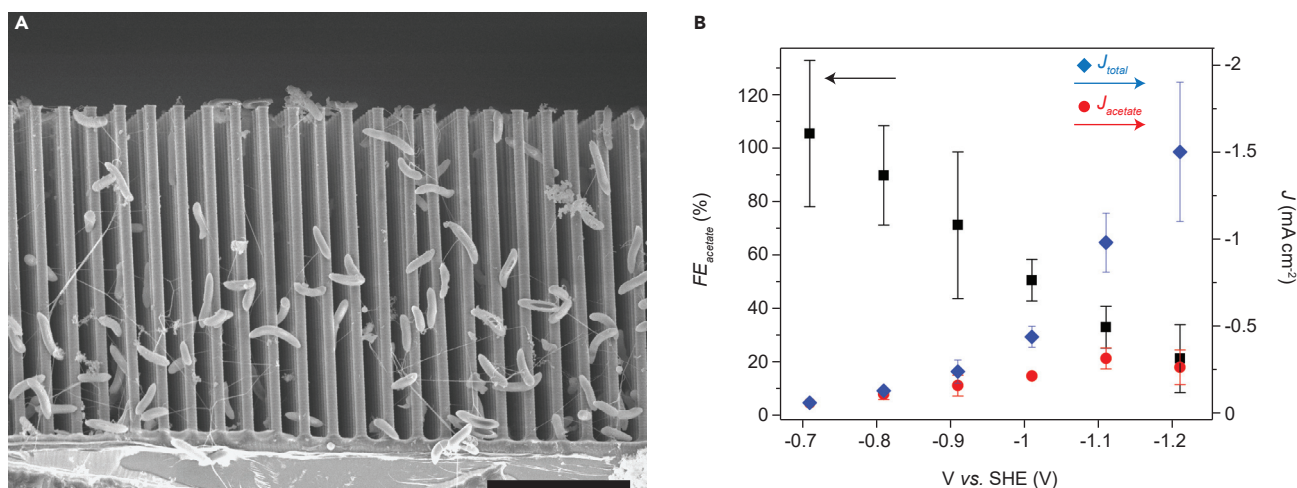


Figure 2. The Imaging and Electrochemical Characterizations of Nanowire-Bacteria Hybrids before Optimization

(A) SEM image of the nanowire-bacteria hybrids (fixed at -0.81 V versus SHE) with standard electrolyte (initial pH value of 7.2) and 4% v/v bacteria inoculation.

(B) The electrochemical performance of the nanowire-bacteria hybrids at different η (starting from less negative η , $n = 3$). J_{acetate} is defined as J_{total} (Figure S3) multiplied by FE_{acetate} . Scale bar, 10 μm .

This system was then subjected to sequentially elevated η from -0.71 V to -1.21 V versus SHE. At low η from -0.71 V to -0.81 V versus SHE, FE_{acetate} was close to 100% (Figure 2B), indicating that the loaded bacteria could efficiently utilize a small flux of reducing equivalents to produce acetate. For example, at -0.81 V versus SHE, the system achieved FE_{acetate} of $91\% \pm 19\%$, and J_{acetate} of $\sim 0.1 \text{ mA cm}^{-2}$ that corresponds to an acetate turnover rate (TOR) of $\sim 1.2 \times 10^6$ acetate molecules per second per cell ($\text{s}^{-1} \text{ cell}^{-1}$). Our calculation is consistent with previous reported TOR of $1.0 \pm 0.3 \times 10^6$ acetate molecules $\text{s}^{-1} \text{ cell}^{-1}$.¹³ However, simply applying a more negative η did not correspondingly increase the acetate production rate. As we further increased the potential and thus the total current, FE_{acetate} dramatically decreased and J_{acetate} plateaued at $\sim 0.3 \text{ mA cm}^{-2}$ (Figure 2B). Specifically, only a 20% FE_{acetate} could be achieved when the total current density (J_{total}) reached $\sim 1.2 \text{ mA cm}^{-2}$. This suggests that a majority of electrons were lost to H_2 evolution (Figure 1) instead of being directly taken up by the *S. ovata*. In addition, despite a high J_{total} , the peak J_{acetate} of $\sim 0.3 \text{ mA cm}^{-2}$ is only comparable with the previously reported value.¹³ This CO_2 -fixation rate limit motivated our efforts to investigate the cause of the mismatched electron flux at the bioinorganic interface. Through thorough scanning electron microscopy (SEM) imaging, we found that the bacteria-electrode interface deteriorated after electrochemical operation at -1.21 V versus SHE. We observed large precipitates on the electrode surface (Figures S4A and S4B), possibly stemming from the inorganic compounds in the electrolyte. Energy-dispersive X-ray spectroscopy confirmed that the precipitates were mainly composed of calcium phosphate and magnesium phosphate (Figure S4C). This is triggered by high pH near the cathode surface due to accelerated proton consumption and inadequate mass transport at high current densities. Increases in local pH have been reported in bioelectrosynthesis as a driving factor for low production rates.^{25–27} Methods to inspect pH microenvironments, such as colorimetric dyes²⁸ have been investigated. However, as our nanostructured electrode complicates common pH measurements, we employed numerical 2D simulations, which reveal that the pH around nanowires increases to ~ 9.3 (Figure S5). The alkaline environment not only brought about the formation of bulky precipitates but also created an incompatible

environment for the biocatalysts.^{27,29} Altogether, this prevented the attachment of *S. ovata* to the electrode (Figure S4) and thus impeded direct extracellular electron transfer (Figure 1), thereby lowering the overall CO₂ conversion rate.¹⁸ In addition, the negatively charged electrode surface under alkaline condition^{30,31} could further deter adhesion of gram-negative *S. ovata*.^{32,33} Based on these findings, we increased the buffer capacity (5× phosphate concentration, initial pH 7.2, denoted as phosphate-enhanced media) to mitigate the pH increase around the nanowire cathode.¹³ However, enhancing the buffer capacity insignificantly improved the system's performance compared with that of the original electrolyte (Figure S6A). At this point, we observed that the *S. ovata* persistently escaped from the nanowire array and formed a biofilm on top after operation at −1.21 V versus SHE (Figures S6B and S6C). This observation implies that the local pH environment at high bias is still biologically unfavorable. Furthermore, evolved H₂ may delaminate *S. ovata* from the nanowire electrode.³⁴ Conclusively, these factors contribute to an obstinately poor bacteria-nanowire interface unable to maintain direct charge uptake at high η .

The formation of a biofilm suggests that the total amount of bacteria increased over the duration of the electrochemical experiment with the phosphate-enhanced electrolyte (Figures S6B and S6C), in contradistinction to the sparsely populated initial electrode. Chadwick et al. previously verified that the most metabolically active bacteria in current-producing biofilms are those directly interfacing the electrode.³⁵ This could explain that although a biofilm forms, only those cells closely contacting the nanowires are robustly undertaking acetogenesis. In addition, Zhang et al. proposed that a close microbe-electrode interaction can increase the microbial CO₂-reducing rate.¹⁸ Therefore, it is imperative to devise a strategy to allow the bacteria to inhabit the nanowire array to fully take advantage of the large electrode surface area. Based on our simulation results, we found that the electrolyte with initial pH of 7.2 leads to a slightly basic environment (pH > 9, at ∼−1.2 V versus SHE) at the electrode interface, whereas an electrolyte with initial pH of 6.4 could more effectively mitigate the local pH change at a potential of ∼−1.2 V versus SHE (Figure 3A). Therefore, we hypothesized that a combination of increased buffering capacity and initial lower electrolyte pH could support a robust bacteria-nanowire interface.

We monitored the development of *S. ovata* within the nanowire arrays over time (Figure S7) employing an enhanced electrolyte with initial pH of 6.4. In order to facilitate the formation of a fully embedded nanowire-bacteria system and thus allow more bacteria to contribute to acetate production, we inoculated the cathodic chamber with a higher concentration of bacteria initially (20% v/v at OD₅₄₅ of 0.38; Figure S1). After inoculation, the system was set at −0.8 V versus SHE, and the current density was maintained at 0.1 to 0.2 mA cm^{−2}, in order to provide a mild electrochemical environment that the bacteria can become accustomed to. Consequently, a close-packed nanowire-bacteria electrode was formed after a 3-day ramp-up stage with a bacteria density of ∼13 cells per nanowire (Figure S8).

Acetate production from CO₂ on this fully embedded nanowire-bacteria system was evaluated at a series of sequentially increasing η . Phosphate-enhanced electrolytes with three different initial pH values (6.4, 6.7, and 7.2) were used to systematically ascertain the influence of local pH at the electrode interface. The optimized hybrid system with different electrolyte pH all exhibited significantly enhanced J_{acetate} (Figure 3B) and FE_{acetate} (Figure 3C) at high η compared with the initial results (Figure 2B). The improvement was due to increased electron uptake by the densely packed biocatalysts around the nanowire electrodes. For all three electrolytes,

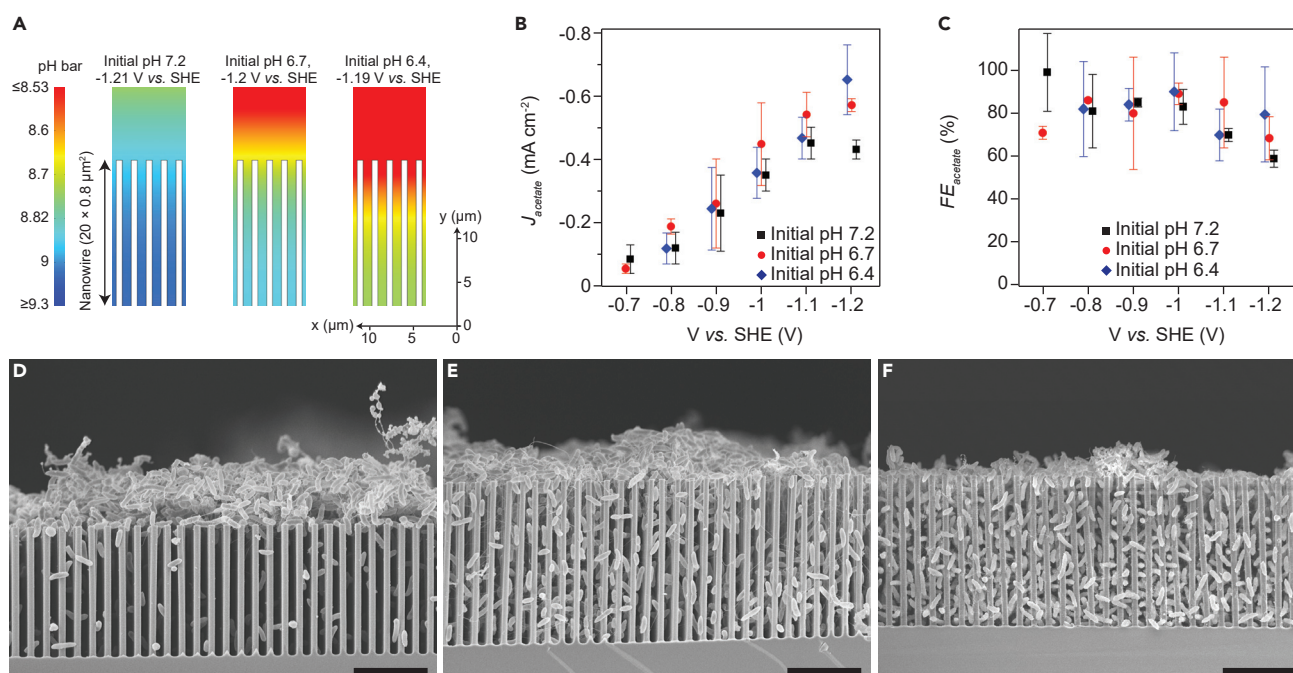


Figure 3. The Electrochemical Performance and SEM Images of Nanowire-Bacteria Hybrids with Optimized Bacteria Loading and Electrolyte Composition

(A) Numerical simulations demonstrate that the transition of initial pH values of phosphate-enhanced electrolytes from 7.2, 6.7, to 6.4 gradually lowered the pH around the nanowires from >9 to <8.7 . The boundary pH values in the simulations were determined by the experimentally measured bulk pH values in the cathode chamber (Figure S9).

(B and C) Bias-dependent J_{acetate} (B) and FE_{acetate} (C) of the fully embedded nanowire-bacteria hybrids using phosphate-enhanced electrolytes with different initial pH values ($n = 3$ for each case).

(D–F) The SEM images of the fully embedded nanowire-bacteria hybrids after operation at ~ -1.2 V versus SHE using electrolytes with different initial pH values. A clear transition from a top aggregation of bacteria (initial pH value of 7.2; D) to a semi-close-packed structure (initial pH value of 6.7; E), and finally to a close-packed structure (initial pH value of 6.4; F) was observed. Scale bar, 10 μm .

FE_{acetate} is maintained around 60%–80% at potentials from -1.0 to -1.2 V versus SHE. These results are considerably higher than those of the unoptimized system (Figure 2B, 20%–50%) where initially *S. ovata* was only sparsely distributed around the electrodes. Correspondingly, the peak J_{acetate} was also increased from ~ 0.3 mA cm^{-2} to >0.45 mA cm^{-2} . For potentials ranging from -0.7 V to -1.1 V versus SHE, the enhanced electrolyte with an initial pH of 6.7 supports the consistently greatest rate of CO_2 -to-acetate conversion, whereas the performance of the electrolytes with initial pH of 6.4 and 7.2 is similar. These results suggest that the electrolyte with initial pH 6.7 can sustain an optimal local microenvironment (including pH and preservation of nickel (Ni) catalyst; Figure S10) for *S. ovata* during operating conditions up to -1.1 V versus SHE. Furthermore, the electrolyte with initial pH of 6.4 has a more compelling effect at ~ -1.2 V versus SHE, allowing for the greatest J_{acetate} . SEM inspection after electrochemical operation at ~ -1.2 V versus SHE revealed that the bacteria resided on top of electrodes, partially inside the nanowire arrays and were densely embedded within the nanowire arrays for electrolytes with initial pH values of 7.2, 6.7, and 6.4, respectively (Figures 3D–3F). The different bacteria-nanowire associations are consistent with our simulation results (Figure 3A) and indicate that the microbes migrate to their favorable environment under different electrochemical conditions. Correspondingly, the peak J_{acetate} at ~ -1.2 V versus SHE was boosted from 0.45 ± 0.05 mA cm^{-2} to 0.57 ± 0.02 mA cm^{-2} and finally up to 0.65 ± 0.11 mA cm^{-2} for electrolytes with initial pH values of 7.2, 6.7, and 6.4,

respectively (Figure 3B). The improved peak J_{acetate} for initial pH 6.4 suggests that the close-packed bacteria-nanowire interface enhanced electron uptake, as evidenced by the FE_{acetate} at ~ -1.2 V versus SHE (Figure 3C). pH lower than 6.2 may dissolve the nickel coating on the electrode, and therefore, the electrolyte pH was not further lowered (Figure S10).

The well-preserved bacteria-nanowire interface (Figure 3F) allowed us to precisely estimate the bacteria density and thus calculate the TOR per bacterium at high η . At a CO_2 -reducing rate of $0.65 \pm 0.11 \text{ mA cm}^{-2}$ with potential of -1.19 V versus SHE, the TOR of *S. ovata* was $1.7 \pm 0.5 \times 10^6$ acetate molecules $\text{s}^{-1} \text{ cell}^{-1}$. For potentials higher than -1.2 V versus SHE, we observed more hydrogen formation leading to a much reduced FE_{acetate} (Figure S11). Altogether these results indicate that a potential of ~ -1.2 V versus SHE yielded a maximum CO_2 -reducing current density of $0.65 \pm 0.11 \text{ mA cm}^{-2}$ under an optimized system with enhanced bacteria loading and a more bio-compatible local pH.

Following the optimization of our microbial electrochemical system we investigated whether our improvements would allow for efficient and sustained solar-to-chemical production.^{7–11,13,36,37} We coupled our close-packed nanowire-bacteria system with a photovoltaic device, as shown in the schematic diagram (Figure 4A) and assessed long-term solar-driven CO_2 -to-acetate production. The two-electrode electrochemical measurement with the close-packed hybrid system showed an onset voltage of ~ 1.8 V, and an ~ 3.2 V operating voltage was needed to reach a current density of $\sim 1 \text{ mA cm}^{-2}$ (Figure 4B). Therefore, we employed a low-cost multi-junction Si solar cell (V_{oc} 4.7 V, I_{sc} 4.4 mA under one sun illumination) to provide enough voltage to drive the overall reaction. The expected operating current density of the integrated platform was determined by the intersection of the J-V curves of both the solar cell (25 mW cm^{-2} , AM 1.5 G illumination) and the hybrid system in a two-electrode configuration (Figure 4B). The resulting value of $\sim 0.82 \text{ mA cm}^{-2}$ matches the optimal total current density found in the electrochemical experiments (Figure S12).

The system was found to steadily produce acetate over 1 week, with daily solar-to-acetate efficiencies between 3% and 4% and an average acetate production rate of $44.3 \text{ g m}^{-2} \text{ day}^{-1}$ or $0.3 \text{ g L}^{-1} \text{ day}^{-1}$ (Figure 4C). Control ^{13}C experiments confirmed the carbon source (Figure S13) and a dark control experiment showed negligible acetate production (Figure S14). The average 3.6% solar-to-acetate efficiency over 7 days corresponds to an average CO_2 -reducing current of 0.65 mA cm^{-2} , which is consistent with electrochemical measurements (Figures 3B and S15). Overall, our results demonstrate a general route to improve the efficiency of bio-electrochemical CO_2 fixation by optimizing the bioinorganic interface. We namely show that a close bioinorganic interface plays a critical role in direct electron uptake in our model system. The insights obtained from this work can be combined with complementary approaches, such as bacteria adaptation,^{19,20} to further improve the CO_2 conversion rate and solar-to-chemical efficiency.

EXPERIMENTAL PROCEDURES

Preparation of p^+ Si Nanowire Array Electrode

p^+ Si nanowire arrays were fabricated using reactive-ion etching of patterned single-crystalline Si wafers.¹³ The 6-inch p^+ -Si wafers ($\rho \sim 0.001\text{--}0.005 \Omega \cdot \text{cm}$) were obtained from Addison Engineering. After thoroughly cleaning in piranha and buffered hydrofluoric acid (BHF), the wafers were patterned with a photoresist dot array using a standard photolithography stepper. Thereafter, the wafers underwent inductive-coupled plasma

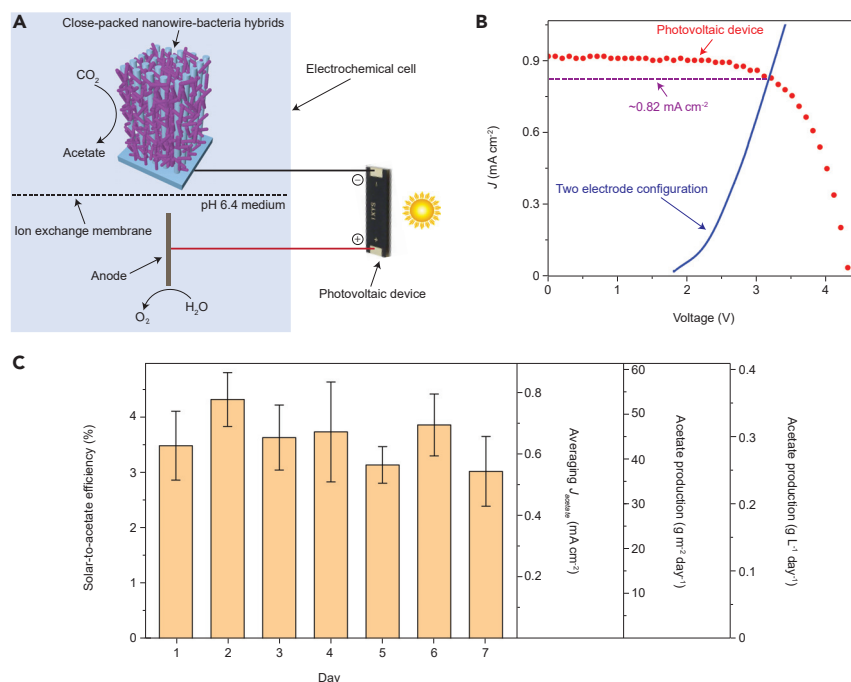


Figure 4. Integrating Close-Packed Nanowire-Bacteria Hybrids with Si Solar Cell for Solar-Driven Acetate Production

(A) Schematic illustration of the integrated device mimicking photosynthesis.

(B) J-V curves of a multi-junction Si solar cell under 25 mW/cm², AM 1.5 G illumination, and the close-packed nanowire-bacteria hybrids in a two-electrode configuration.

(C) The acetate production and solar efficiency of the device over 1 week (n = 3). The four y axes represent (from left to right) the solar-to-acetate energy conversion efficiency, the calculated daily averaging J_{acetate} , the daily acetate production based on electrode projected area, and the daily acetate production per unit volume, respectively.

deep reactive-ion etching (Surface Technology Systems) to yield uniform nanowire arrays (~20 μm long and ~900 nm in diameter). The Si nanowire arrays were thermally oxidized at 1,000°C for 3 h, followed by etching in BHF for at least 5 min. The resulting thinned-down Si nanowires (700–800 nm in diameter) were subsequently coated with 5 nm of TiO₂ protective layer by atomic layer deposition (Picosun ALD), in order to maintain stable performance in a near-neutral pH electrolyte for a long period of time. To facilitate the electron transfer from the cathode to the bacterium *S. ovata*,¹⁸ ~10 nm nickel (Ni) was sputtered at the surface of the resulting Si nanowire arrays (Edwards). For the electrode fabrication, ohmic contact to the device chip was made by rubbing Ga-In eutectic on its back side. Thereafter, the chip was fixed on Ti foil with conductive silver paint and carbon tape, resulting in good electrical connections. After that, the Si nanowire array samples were sealed using nail polish, and the electrodes were ready for electrochemical characterizations.

Electrochemical Characterization

S. ovata (DSM 2662) was originally obtained from the American Type Culture Collection. An inoculum of *S. ovata* was grown in DSMZ 311 medium (betaine, casitone, and resazurin omitted; yeast extract added) under strict anaerobic conditions with hydrogen as the electron donor (80% H₂ and 20% CO₂), as previous work described.^{12,13,18} After 6 days of growth, the OD₅₄₅ reached 0.372 ± 0.012 (Figure S1), and such hydrogen-grown bacteria were ready for subsequent electrochemical CO₂ fixation. All electrochemical measurements were carried out using a home-built electrochemical setup.

The setup is a two-chamber cell, with the working electrode and reference electrode (Ag/AgCl, 1 M KCl, CH Instruments) in one chamber and a Pt wire as counter electrode in the other chamber. The two chambers were separated by a proton-exchange membrane (Nafion 212, FuelCellStore) when standard medium^{12,18} was used as the electrolyte. The nafion membrane was replaced by an anion-exchange membrane (AMI-7001S, kindly provided by Membranes International) when phosphate-enhanced medium¹³ was used as the electrolyte, to facilitate the mass transport of the negatively charged phosphate buffer ions and bicarbonate ions. The electrochemical characterization was performed using Gamry Interface 1000 potentiostats. Because of the change of the local pH over the entire experiment, FE_{acetate} and J_{acetate} were both characterized versus SHE and were defined as follows:

$$V \text{ versus SHE (V)} = V \text{ versus Ag/AgCl (V)} + 0.209 \text{ (V)}$$

The overpotential η for CO₂ reduction is defined as the voltage difference between the applied electrochemical potential and the standard potential for CO₂ reduction into acetic acid:

$$\eta \text{ (V)} = V \text{ versus RHE (V)} - 0.143 \text{ (V)}$$

Here, RHE is the reversible hydrogen electrode potential defined as

$$V \text{ versus RHE (V)} = V \text{ versus SHE (V)} + 0.059 \times \text{pH}$$

The nanowire-bacteria hybrids were realized in the cathode chamber using an organic-free minimal medium. Standard medium and phosphate-enhanced medium were both used as the electrolytes, to obtain different levels of proton mass transport, as mentioned above. For the phosphate-enhanced electrolyte, the initial pH value of the electrolyte was systematically tuned from 7.2 to 6.7 and finally 6.4, by adding a certain amount of hydrochloric acid. The electrolyte was introduced to the electrochemical cell until its pH value was completely stabilized. We first ran abiotic chronoamperometry (−0.8 V versus SHE) for 24 h before bacteria inoculation in order to allow the inert gas bubbling to remove O₂ residue in the cathode chamber. The hydrogen-grown *S. ovata* cells were then inoculated into the cathode chamber (4% v/v at OD₅₄₅ of 0.38 for unoptimized system, and 20% v/v at OD₅₄₅ of 0.38 for optimized system). The inoculation v/v ratio was adjusted accordingly if the OD₅₄₅ slightly differed from 0.38. After bacteria inoculation, the electrochemical bias was kept at −0.8 V versus SHE, and the dispersion was cultured under 80% N₂/10% H₂/10% CO₂ gas environment for 24 h. At this stage, the electrolyte in the cathode chamber was turbid due to suspended bacteria. The bubbling gas was then switched to 80% N₂/20% CO₂. At this stage the electrochemical bias (−0.8 V versus SHE) was maintained, and the Si nanowire electrode served as the sole electron source for the bacteria metabolism. The current density was maintained at ~0.15 mA cm^{−2} in order to provide a mild electrochemical environment for the bacteria to become accustomed to. After 24-h incubation under 80% N₂/20% CO₂, half of the electrolyte in the cathode chamber was carefully replaced with fresh medium. After one more cycle of such medium exchange, the electrolyte in the cathode chamber became clear as most bacteria settled within the nanowire arrays, and a stable bacteria-nanowire interface was achieved. Next, the hybrids were ready for electrochemical acetate production as follows.

Analysis of Acetate Production

Starting from less negative η , chronoamperometry was run for at least 12 h at each electrochemical bias. After one chronoamperometry cycle was complete, an aliquot

of the medium was sampled and a same amount of fresh medium was injected into the electrochemical cell. When nafion membrane was used, aliquots were only sampled from the cathode chamber for acetate analysis. In addition, aliquots were sampled from both the cathode chamber and anode chamber for acetate analysis when anion-exchange membrane was used. Acetate concentration of the sample was quantified by proton nuclear magnetic resonance (^1H -qNMR) spectroscopy with sodium 3-(trimethylsilyl)-2,2',3,3'-tetradeuteriopropionate (TMSP-d4) as the internal standard. For the isotope labeling experiment, ^{13}C -labeled bicarbonate was used, and the same protocol was applied (Figure S13). After obtaining the acetate concentration of each sample, FE_{acetate} was calculated based on following equation:

$$FE_{\text{acetate}} = \frac{96485 \times 8 \times \text{incremental mole of acetic acid}}{\int I dt},$$

and the specific CO_2 -reducing current density J_{acetate} is defined as follows:

$$J_{\text{acetate}} = FE_{\text{acetate}} \times J_{\text{total}},$$

where J_{total} is the stabilized total current density during chronoamperometry (Figure S3). In addition to acetate production, the electrons can be also used to produce biomass and H_2 . As a result,

$$FE_{\text{acetate}} + FE_{\text{biomass}} + FE_{\text{H}_2} = 1.$$

Scanning Electron Microscopy Characterization

After the electrochemical characterizations were complete, the nanowire-bacteria hybrids were subjected to SEM characterization. First, an overnight bacteria fixation was performed by adding 2.5% glutaraldehyde directly to the medium in the cathode chamber.³⁸ Then the electrodes were washed with de-ionized water, followed by dehydration in increasing concentrations of ethanol (12.5%, 25%, 37.5%, 50%, 62.5%, 75%, 87.5%, and 100%, 15 min each). Critical point drying (Tousimis) was used to dry the nanowire-bacteria samples in order to minimize the effect of the capillary force. Prior to imaging, the electrodes were cleaved along the middle and then sputtered with ~ 5 nm Au (Denton Vacuum, LLC). The nanowire-bacteria hybrids were imaged at 5 keV/12 μA by field emission SEM (JEOL FSM6430). The density of *S. ovata* could be precisely estimated for the SEM image that showed clear bioinorganic interface. For the sparsely populated hybrids (Figure 2A), the cell density was calculated by counting the number of cells within given areas of SEM images (Figure S2). For the close-packed hybrids, the cell density was estimated by multiplying the density along the z axis by the density over the x-y plane, as shown in Figure S8.

Numerical Simulation

The local pH within the nanowire arrays was simulated using the Electrochemical Module (steady state) of the COMSOL Multiphysics finite-element-analysis software package. In the 2D simulations, the nanowire's geometry (20 μm long, 0.8 μm in diameter, and 2 μm pitch) is consistent with the experiment. To simplify the model geometry, we use five nanowires to represent the whole nanowire arrays (Figure 3A). Both phosphate buffer (H_3PO_4 , H_2PO_4^- , HPO_4^{2-} , and PO_4^{3-}) and bicarbonate buffer (H_2CO_3 , HCO_3^- , and CO_3^{2-}) were accounted in the simulation. In the simulation, the mass transport is governed by the diffusion of ion species. At the nanowire's surface, the proton consumption rate is governed by the Tafel equation,³⁹ which is as follows:

$$i = i_0 e^{\frac{-\alpha F \eta}{RT}},$$

where i_0 (exchange current density) and α (transfer coefficient) were both extracted from the experimental Tafel plot. Transfer of one electron corresponds to consumption of one proton. As high-concentration supporting ions were present in the actual electrolyte, the ion migration was not considered in this simulation. The stirring-induced convection was simplified into a diffusion layer model, and the diffusion layer thickness (δ) was assumed to be 50 μm for all the involved ions.^{40,41} Beyond the diffusion layer, the concentrations of all the ions were constant determined by the boundary conditions. The boundary pH value was determined by the experimentally measured bulk pH value in the cathode chamber. Within the diffusion layer, the ion mass transport was governed by Fick's law. The diffusion coefficients of all ion species were obtained from the literature.³⁹ The equilibrium equations of the buffer systems applied to all the domains. All equilibrium constants were obtained from the literature.³⁹ The minimum domain mesh size in the simulation was set to be 0.05 μm .

Solar-Driven Acetate Production

For the solar-driven acetate production, a two-electrode configuration was used,⁴² where the nanowire-bacteria hybrids worked as the cathode and a Pt wire acted as the anode. Phosphate-enhanced medium (organic free, initial pH of 6.4) was used as the electrolyte. With the applied electrochemical bias maintained at -3.2 V , the hydrogen-grown *S. ovata* cells (20% v/v inoculum at OD₅₄₅ of 0.38) were introduced into the cathode chamber, where the dispersion was first purged with 80%N₂/10%H₂/10%CO₂ gas mixture for 24 h. The gas environment was then switched to 80%N₂/20%CO₂, and half of the electrolyte was replaced with fresh medium every 24 h (repeated twice), similar to the electrochemical measurements mentioned above. After such medium exchange process, the established nanowire-bacteria hybrids were ready for the solar-driven acetate production. A commercial single-crystalline Si solar cell (KXOB22-01X8F) was obtained from Digikey Corporation. A 300W Xenon arc lamp (Newport Corporation) with an AM 1.5 G filter was used for illumination, and the light intensity (25 mW cm^{-2}) was calibrated using a Si photodiode referenced to an NREL-calibrated Si photodiode. Once the solar cell was connected to the electrodes, an aliquot of the medium was sampled every 24 h for acetate quantification, and a same amount of fresh medium was injected into the electrochemical cell. The solar acetate production lasted for 7 days. The daily solar-to-acetate efficiency (ξ) was calculated based on the following equation:

$$\xi = \frac{8 \times 1.09(\text{V}) \times N_{\text{acetate}}(\text{mol}) \times 96,485(\text{C mol}^{-1})}{I(\text{mW cm}^{-2}) \times A_{\text{sc}}(\text{cm}^2) \times 24 \times 3,600(\text{s})} \times 100\%,$$

where 8 represents the number of electrons needed to produce one acetate molecule, 1.09 V is the thermodynamic potential needed to reduce CO₂ into acetate,¹³ N_{acetate} is the amount of acetate produced in 1 day, I is the light intensity (25 mW cm^{-2}), and A_{sc} is the projected area of the Si solar cell (0.96 cm^2). Alternatively, ξ can also be expressed based on the calculated averaging J_{acetate} as follows:

$$\xi = \frac{1.09(\text{V}) \times \text{Averaging } J_{\text{acetate}}(\text{mA cm}^{-2}) \times A_{\text{electrode}}}{I(\text{mW cm}^{-2}) \times A_{\text{sc}}(\text{cm}^2)} \times 100\%,$$

where $A_{\text{electrode}}$ is the projected area of our Si nanowire electrode (1.2 cm^2).

SUPPLEMENTAL INFORMATION

Supplemental Information can be found online at <https://doi.org/10.1016/j.joule.2020.03.001>.

ACKNOWLEDGMENTS

This work was supported by the National Aeronautics and Space Administration (NASA), under grant number NNX17AJ31G. The authors would like to acknowledge Dr. Long Hu, Dr. Kelsey Sakimoto, Dr. Hao Liu, Dr. Yingbo Zhao, Dr. Yifan Li, Tom Tacken, Anthony Abel, Mathangi Soundararajan, and Aaron Berliner for helpful discussions. The authors thank the Marvell Nanofabrication Laboratory for use of their facilities. Y.S. acknowledges the graduate fellowship support from USTC-Suzhou Industrial Park. S.C.-B. thanks the Philomathia Foundation.

AUTHOR CONTRIBUTIONS

Y.S. and P.Y. designed the experiments. Y.S., S.C.-B., and Q.K. fabricated the silicon nanowire electrodes. Y.S., S.C.-B., J.M.K., Y.-x.S., and C.L. performed the bacteria culturing and incubation. Y.S., S.C.-B., J.M.K., Y.-x.S., and H.Z. conducted the electrochemical and solar-driven experiments. Y.S., D.L., and Y.C. performed the numerical calculation. Y.S., S.C.-B., Y.-x.S., and P.Y. co-wrote the paper. All authors discussed the results and revised the manuscript.

DECLARATION OF INTERESTS

The authors declare no competing interests.

Received: December 18, 2019

Revised: February 17, 2020

Accepted: February 29, 2020

Published: March 31, 2020

REFERENCES

- Chiappini, C., De Rosa, E.D., Martinez, J.O., Liu, X., Steele, J., Stevens, M.M., and Tasciotti, E. (2015). Biodegradable silicon nanoneedles delivering nucleic acids intracellularly induce localized in vivo neovascularization. *Nat. Mater.* **14**, 532–539.
- Sharei, A., Zoldan, J., Adamo, A., Sim, W.Y., Cho, N., Jackson, E., Mao, S., Schneider, S., Han, M.J., Lytton-Jean, A., et al. (2013). A vector-free microfluidic platform for intracellular delivery. *Proc. Natl. Acad. Sci. USA* **110**, 2082–2087.
- Tian, B., Cohen-Karni, T., Qing, Q., Duan, X., Xie, P., and Lieber, C.M. (2010). Three-dimensional, flexible nanoscale field-effect transistors as localized bioprobes. *Science* **329**, 830–834.
- Xie, C., Lin, Z., Hanson, L., Cui, Y., and Cui, B. (2012). Intracellular recording of action potentials by nanopillar electroporation. *Nat. Nanotechnol.* **7**, 185–190.
- Logan, B.E. (2009). Exoelectrogenic bacteria that power microbial fuel cells. *Nat. Rev. Microbiol.* **7**, 375–381.
- Lovley, D.R. (2006). Bug Juice: harvesting electricity with microorganisms. *Nat. Rev. Microbiol.* **4**, 497–508.
- Sakimoto, K.K., Wong, A.B., and Yang, P. (2016). Self-photosensitization of nonphotosynthetic bacteria for solar-to-chemical production. *Science* **351**, 74–77.
- Zhang, H., Liu, H., Tian, Z., Lu, D., Yu, Y., Cestellos-Blanco, S., Sakimoto, K.K., and Yang, P. (2018). Bacteria photosensitized by intracellular gold nanoclusters for solar fuel production. *Nat. Nanotechnol.* **13**, 900–905.
- Nichols, E.M., Gallagher, J.J., Liu, C., Su, Y., Resasco, J., Yu, Y., Sun, Y., Yang, P., Chang, M.C.Y., and Chang, C.J. (2015). Hybrid bioinorganic approach to solar-to-chemical conversion. *Proc. Natl. Acad. Sci. USA* **112**, 11461–11466.
- Liu, C., Colón, B.C., Ziesack, M., Silver, P.A., and Nocera, D.G. (2016). Water splitting–biosynthetic system with CO₂ reduction efficiencies exceeding photosynthesis. *Science* **352**, 1210–1213.
- Zhang, T. (2015). More efficient together. *Science* **350**, 738–739.
- Nevin, K.P., Woodard, T.L., Franks, A.E., Summers, Z.M., and Lovley, D.R. (2010). Microbial electrosynthesis: feeding microbes electricity to convert carbon dioxide and water to multicarbon extracellular organic compounds. *mBio* **1**, 1–4.
- Liu, C., Gallagher, J.J., Sakimoto, K.K., Nichols, E.M., Chang, C.J., Chang, M.C.Y., and Yang, P. (2015). Nanowire-bacteria hybrids for unassisted solar carbon dioxide fixation to value-added chemicals. *Nano Lett.* **15**, 3634–3639.
- Rabaey, K., and Rozendal, R.A. (2010). Microbial electrosynthesis—revisiting the electrochemical route for microbial production. *Nat. Rev. Microbiol.* **8**, 706–716.
- Lewis, N.S., and Nocera, D.G. (2006). Powering the planet: chemical challenges in solar energy utilization. *Proc. Natl. Acad. Sci. USA* **103**, 15729–15735.
- Marshall, C.W., Ross, D.E., Fichot, E.B., Norman, R.S., and May, H.D. (2013). Long-term operation of microbial electrosynthesis systems improves acetate production by autotrophic microbiomes. *Environ. Sci. Technol.* **47**, 6023–6029.
- Cui, M., Nie, H., Zhang, T., Lovley, D.R., and Russell, T.P. (2017). Three-dimensional hierarchical metal oxide–carbon electrode materials for highly efficient microbial electrosynthesis. *Sustain. Energy Fuels* **1**, 1171–1176.
- Zhang, T., Nie, H., Bain, T.S., Lu, H., Cui, M., Snoeyenbos-West, O.L., Franks, A.E., Nevin, K.P., Russell, T.P., and Lovley, D.R. (2013). Improved cathode materials for microbial electrosynthesis. *Energy Environ. Sci.* **6**, 217–224.
- Ammam, F., Tremblay, P.L., Lizak, D.M., and Zhang, T. (2016). Effect of tungstate on acetate and ethanol production by the electrosynthetic bacterium *Sporomusa ovata*. *Biotechnol. Biofuels* **9**, 163.
- Tremblay, P.L., Höglund, D., Koza, A., Bonde, I., and Zhang, T. (2015). Adaptation of the autotrophic acetogen *Sporomusa ovata* to

- methanol accelerates the conversion of CO₂ to organic products. *Sci. Rep.* 5, 16168.
21. Patil, S.A., Arends, J.B.A., Vanwonterghem, I., van Meerbergen, J.V., Guo, K., Tyson, G.W., and Rabaey, K. (2015). Selective enrichment establishes a stable performing community for microbial electrosynthesis of acetate from CO₂. *Environ. Sci. Technol.* 49, 8833–8843.
 22. Su, Y., Liu, C., Brittman, S., Tang, J., Fu, A., Kornienko, N., Kong, Q., and Yang, P. (2016). Single-nanowire photoelectrochemistry. *Nat. Nanotechnol.* 11, 609–612.
 23. Liu, M., Pang, Y., Zhang, B., De Luna, P., Voznyy, O., Xu, J., Zheng, X., Dinh, C.T., Fan, F., Cao, C., et al. (2016). Enhanced electrocatalytic CO₂ reduction via field-induced reagent concentration. *Nature* 537, 382–386.
 24. Ross, M.B., De Luna, P., Li, Y., Dinh, C.T., Kim, D., Yang, P., and Sargent, E.H. (2019). Designing materials for electrochemical carbon dioxide recycling. *Nat. Catal.* 2, 648–658.
 25. LaBelle, E.V., and May, H.D. (2017). Energy efficiency and productivity enhancement of microbial electrosynthesis of acetate. *Front. Microbiol.* 8, 756.
 26. Jourdin, L., Freguia, S., Flexer, V., and Keller, J. (2016). Bringing high-rate, CO₂-based microbial electrosynthesis closer to practical implementation through improved electrode design and operating conditions. *Environ. Sci. Technol.* 50, 1982–1989.
 27. Mohanakrishna, G., Seelam, J.S., Vanbroekhoven, K., and Pant, D. (2015). An enriched electroactive homoacetogenic biocathode for the microbial electrosynthesis of acetate through carbon dioxide reduction. *Faraday Discuss.* 183, 445–462.
 28. Qu, F., Li, N.B., and Luo, H.Q. (2013). Highly sensitive fluorescent and colorimetric pH sensor based on polyethylenimine-capped silver nanoclusters. *Langmuir* 29, 1199–1205.
 29. Möller, B., Ossmer, R., Howard, B.H., Gottsechalk, G., and Hippe, H. (1984). *Sporomusa*, a new genus of gram-negative anaerobic bacteria including *Sporomusa sphaeroides* spec. nov. and *Sporomusa ovata* spec. nov. *Arch. Microbiol.* 139, 388–396.
 30. Holmberg, J.P., Ahlberg, E., Bergenholtz, J., Hassellöv, M., and Abbas, Z. (2013). Surface charge and interfacial potential of titanium dioxide nanoparticles: experimental and theoretical investigations. *J. Colloid Interface Sci.* 407, 168–176.
 31. Preočanin, T., and Kallay, N. (2006). Point of zero charge and surface charge density of TiO₂ in aqueous electrolyte solution as obtained by potentiometric mass titration. *Croat. Chem. Acta* 79, 95–106.
 32. Sára, M., and Sleytr, U.B. (2000). S-layer proteins. *J. Bacteriol.* 182, 859–868.
 33. Beveridge, T.J. (1999). Structures of gram-negative cell walls and their derived membrane vesicles. *J. Bacteriol.* 181, 4725–4733.
 34. Blanchet, E., Duquenne, F., Rafrati, Y., Etcheverry, L., Erable, B., and Bergel, A. (2015). Importance of the hydrogen route in up-scaling electrosynthesis for microbial CO₂ reduction. *Energy Environ. Sci.* 8, 3731–3744.
 35. Chadwick, G.L., Jiménez Otero, F.J., Gralnick, J.A., Bond, D.R., and Orphan, V.J. (2019). NanoSIMS imaging reveals metabolic stratification within current-producing biofilms. *Proc. Natl. Acad. Sci. USA* 116, 20716–20724.
 36. Zhang, J.Z., Bombelli, P., Sokol, K.P., Fantuzzi, A., Rutherford, A.W., Howe, C.J., and Reisner, E. (2018). Photoelectrochemistry of photosystem II *in vitro* vs. *in vivo*. *J. Am. Chem. Soc.* 140, 6–9.
 37. Kornienko, N., Zhang, J.Z., Sakimoto, K.K., Yang, P., and Reisner, E. (2018). Interfacing nature's catalytic machinery with synthetic materials for semi-artificial photosynthesis. *Nat. Nanotechnol.* 13, 890–899.
 38. Sakimoto, K.K., Liu, C., Lim, J., and Yang, P. (2014). Salt-induced self-assembly of bacteria on nanowire arrays. *Nano Lett.* 14, 5471–5476.
 39. Bard, A.J., and Faulkner, L.R. (2000). *Electrochemical Methods: Fundamentals and Applications*, Second Edition (John Wiley & Sons).
 40. Walker, R., and Holt, N.S. (1984). Determination of the Nernst diffusion layer thickness in the hydrosol agitation tank. *Surf. Technol.* 22, 165–174.
 41. Tobias, C.W., Eisenberg, M., and Wilke, C.R. (1952). Diffusion and convection in electrolysis—a theoretical review. *Electrochem. Ionic Cryst.* 99, 359–365.
 42. Luo, J., Im, J.H., Mayer, M.T., Schreier, M., Nazeeruddin, M.K., Park, N.G., Tilley, S.D., Fan, H.J., and Grätzel, M. (2014). Water photolysis at 12.3% efficiency via perovskite photovoltaics and earth-abundant catalysts. *Science* 345, 1593–1596.
 43. Kumar, A., Hsu, L.H., Kavanagh, P., Barrière, F., Lens, P.N.L., Lapinonnière, L., Lienhard, V.J.H., Schröder, U., Jiang, X., and Leech, D. (2017). The ins and outs of microorganism-electrode electron transfer reactions. *Nat. Rev. Chem.* 1, 24.
 44. Tremblay, P.L., Angenent, L.T., and Zhang, T. (2017). Extracellular electron uptake: among autotrophs and mediated by surfaces. *Trends Biotechnol.* 35, 360–371.